Journal of Power Sources 185 (2008) 570–576

Contents lists available at ScienceDirect

Journal of Power Sources

journal homepage: www.elsevier.com/locate/jpowsour

Influence of polymer concentration and dyes on photovoltaic performance of dye-sensitized solar cell with P(VdF-HFP)-based gel polymer electrolyte

D. Saikia [1], C.C. Han, Y.W. Chen-Yang *

Department of Chemistry, Center for Nanotechnology and R&D Center for Membrane Technology, Chung Yuan Christian University, Chung Li 32023, Taiwan, ROC

ARTICLE INFO

Article history:
Received 24 April 2008
Received in revised form 17 June 2008
Accepted 23 June 2008
Available online 3 July 2008

Keywords:
Dye-sensitized solar cell
Quasi-solid-state polymer electrolyte
Ionic conductivity
Nanocrystalline TiO_2

ABSTRACT

A series of gel polymer electrolytes (GPEs) is synthesized using Poly(vinylidenefluoride-hexafluoropropylene) P(VdF-HFP) as the host matrix and propylene carbonate (PC)–diethyl carbonate (DEC) as plasticizers to fabricate dye-sensitized solar cells. Equal amounts of PC and DEC are used to comprehend high dielectric constant and low viscosity of the electrolyte. The as-prepared GPEs are characterized by XRD, FTIR and SEM. Their thermal properties and ionic conductivities are investigated by TGA/DSC analyses and AC impedance measurements, respectively. The optimized gel polymer electrolyte gives a maximum ionic conductivity of 5.25×10^{-3} S cm^{-1} at room temperature. The formation of porous structure in the electrolyte film supports the entrapment of large volumes of liquid electrolyte inside its cavities. The role of N3 and N719 dyes are also investigated for better photovoltaic performance of DSSC. The overall light-to-electrical-energy conversion efficiencies of 3.95% and 4.41% are obtained for N3 and N719 dyes, respectively, under 100 mW cm^{-2} irradiation, which are comparable to those obtained from the corresponding liquid electrolyte cell.

1. Introduction

The development of renewable energy sources for future energy systems, especially solar energy, has been growing at an ever increasing pace due to global warming and limited availability of fossil fuels. The dye-sensitized solar cell (DSSC) provides an attractive alternative to solid-state photovoltaics for the conversion of solar energy to electricity. This next generation solar cell has received considerable attention due to low manufacturing cost and simple preparation technique over conventional solar cells [1–5]. A photoelectric conversion efficiency of 11% has been achieved in DSSCs with organic solvent-based electrolyte [5]. However, liquid electrolytes create significant technological problems such as leakage, evaporation of solvent, high-temperature instability and flammability, possible desorption and photodegradation of the attached dyes. The corrosion of the Pt counter electrode with such electrolytes also affects the durability of DSSC. All of these demerits limit the practical applications of the DSSCs. Therefore, many attempts have been made to replace liquid electrolytes with quasi-solid/solid-state electrolytes, such as ionic liquid-based gel electrolytes [6–8], gel polymer electrolytes (GPEs) [9–13] and solid polymer electrolytes [14–18]. Although significantly high efficiencies have been accomplished from the solid polymer electrolyte, solvent absence in the electrolyte can easily lead to serious problems, such as crystallization of the iodide salt and, consequently, deterioration of the cell. This problem can be overcome by using gel polymer electrolytes [9–13], which are on the boundary between liquid and solid electrolytes. The polymer matrix acts as a host for a plasticizer which interpenetrates or swells the polymer. Thus, a gel is formed between the plasticizer and the polymer host structure, presenting high boiling point and assuring the non-volatile nature of the electrolyte. Owing to their unique hybrid network structure, gels always possess, simultaneously, both the cohesive properties of solids and the diffusive transport properties of liquids. In addition, the plasticizer, usually a low molar mass polyether (e.g. PEG) or a polar organic solvent (e.g. ethylene carbonate or propylene carbonate), is introduced in small fractions into the polymeric matrix in order to ensure high levels of ion dissociation and thus to provide high ionic conductivity and long life of the cell and offer a satisfactory overall conversion efficiency [19].

In this study, a series of P(VdF-HFP)-based gel polymer electrolytes has been prepared by varying the amount of polymer. It is known that fluorinated polymers are photochemically stable even in the presence of TiO_2 and Pt nanoparticles [20–22], which underlines a potential application of P(VdF-HFP) as a suitable solid-state matrix for redox electrolyte in a long-term stable dye-sensitized solar cell.

* Corresponding author. Tel.: +886 3 2653317; fax: +886 3 2653399.
E-mail address: yuiwhei@cycu.edu.tw (Y.W. Chen-Yang).
[1] Presently at Department of Chemistry, National Central University, Chung-Li, Taiwan.

0378-7753/$ – see front matter.
doi:10.1016/j.jpowsour.2008.06.063

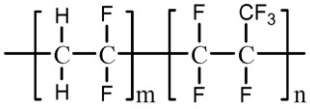

Structure of P(VdF-HFP) co-polymer

2. Experimental

2.1. Materials

Commercial titanium dioxide powder (P25, Degussa) was used as TiO_2 sources. Poly(vinylidenefluoride-hexafluoropropylene) (PVdF-HFP, MW 400,000) and 4-*tert*-butylpyridine (TBP) were obtained from Aldrich Company. LiI and I_2 were purchased from MERCK and STREM Chemicals, respectively. Triton X-100, acetonitrile (ACN) and propylene carbonate (PC) were purchased from ACROS Company. Diethyl carbonate (DEC) was acquired from Lancaster. Polyethylene glycol (PEG) was obtained from Alfa Aesar. The organometallic dye *cis*-bis(isothiocyanato)-bis(2,2′-bipyridyl-4,4′-dicarboxylato)ruthenium(II) (N3) and *cis*-dithiocyanate-*N*,*N*′-bis-(4-carboxylate-4-tetrabutylammonium carboxylate-2,2′-bipyridine) ruthenium(II) (N719) were obtained from Solaronix. Conductive glass substrates (fluorine doped tin oxide overlayer (FTO glass)) with a sheet resistance of 8 Ω cm^{-2} purchased from Solaronix were used as substrates for precipitating porous TiO_2 films. All reagents were used as received.

2.2. Preparation of the sensitized nanocrystalline TiO_2 films

FTO glass substrates were immersed in a saturated solution of KOH in 2-propanol overnight, rinsed with acetone, ethanol and doubly deionized water successively, and dried in a nitrogen stream. TiO_2 colloidal paste was prepared by grinding appropriate amount of TiO_2 nanoparticles together with binder polyethylene glycol (M_w = 20,000) and surfactant Triton-X-100 in ethanol solution. The TiO_2 paste was coated over the FTO glass by doctor-blade technique. The film was sintered in air at 450 °C for 30 min, and then the process repeated to increase the thickness of the film to around 10 μm. Film thickness was measured by Alpha-Step Profilometer testing. When cooling to a temperature of 80–90 °C, the TiO_2 film was sensitized by immersing in ethanol solution containing 0.5 mM N3 or N719 dye for 12 h and then washed with anhydrous ethanol and dried in a oven at 100 °C to get the final TiO_2 film electrode.

2.3. Preparation of polymer gel electrolyte

P(VdF-HFP) as host polymer, lithium iodide/iodine (LiI/I_2) as redox couple, PC and DEC as plasticizers were used to prepare the gel polymer electrolyte. Appropriate amount of P(VdF-HFP) was dissolved in small amount of acetonitrile (ACN). 0.5 M LiI salt and 0.05 M I_2 were dissolved in a mixture of PC and DEC (1:1 (v/v)) separately. It is known that the values of dielectric constants affect the dissolution and separation of ions. High dielectric constants are good for obtaining large amount of charge carriers in electrolyte, which leads to high ionic conductivity [23]. On the other hand, high viscosity causes low ionic conductivity. PC has high dielectric constant (ε = 64.6) but has high viscosity (η = 2.53) also, whereas DEC has low dielectric constant (ε = 2.82) but has low viscosity (η = 0.748). PC + DEC (50% by volume each) solvent was used as a compromise for high dielectric constant ε = 33.71) and low viscosity (η = 1.639) to achieve high ionic conductivity. Both polymer and I^-/I_3^- redox solution were mixed together, stirred, and heated at 60 °C for 1 h. With this solution, 0.5 M 4-*tert*-butylpyridine (TBP) was added and continuously stirred for 24 h at 60 °C. The viscous solution thus obtained was cast onto petri dishes and allowed to dry at room temperature to get the gel polymer electrolyte films.

2.4. Cell assembly

A quasi-solid-state dye-sensitized solar cell was fabricated by clipping dye-sensitized TiO_2 electrode and a platinum counter electrode. The gel polymer electrolyte was introduced slowly into the cell at 60 °C through the aperture between the TiO_2 porous film electrode and a Pt plate electrode. After cooling down to room temperature, a uniform motionless polymer gel layer was formed in cells. Under the pressure of clips, polymer gel electrolyte was inserted into the pores of dye-sensitized TiO_2 nanostructure electrode to form good interfacial contact. The active area of the cell was about 0.25 cm^2.

2.5. Characterization and instruments

Photocurrent–voltage (*J*–*V*) measurements were performed using Autolab's potentiostat/galvanostat instrument and by illuminating the cell through the active photoelectrode, under 500-W Xe light source in combination with standard AM1.5 optical filter. The power of the incident white light from the Xenon lamp was 100 mW cm^{-2}.

The ionic conductivities of the gel polymer electrolytes were obtained using an electrochemical cell consisting of the electrolyte film sandwiched between two stainless steel blocking electrodes and placed in a temperature-controlled oven at vacuum (<10^{-2} Torr). The impedance measurements of the electrolytes films were carried out on HP 4192A impedance analyzer over the frequency range of 5 Hz to 1 MHz in the temperature range 30–80 °C. The XRD patterns of the electrolyte samples were recorded at 45 kV and 40 mA, having a scan step 0.1° using a PANalytical X'Pert PRO X-ray diffractometer. Attenuated total reflection Fourier transform infrared (ATR-FTIR) spectra were recorded at room temperature using a Bio-Rad FTS-7 FTIR system coupled to a computer. The resolution and scan numbers of IR measurement were 2 cm^{-1} and 64 times, respectively. The spectra were collected over the range 400–4000 cm^{-1}. Differential scanning calorimetry (DSC) and thermogravimetric analysis (TGA) of the gel polymer electrolytes were carried out with a Seiko DSC 220C and a Seiko TG/DTA 220, respectively. The samples were heated at a rate of 10 °C min^{-1} under nitrogen flow from −120 to 350 °C for DSC measurement and from 25 to 150 °C for TGA measurement. Approximately 7–10 mg of each sample was weighed and sealed in an aluminium pan for DSC analysis. The surface morphology of the TiO_2 coated film and polymer electrolytes were studied by Hitachi field emission scanning electron microscope (FE-SEM).

3. Results and discussion

3.1. X-ray diffraction

Fig. 1 displays the XRD patterns of P(VdF-HFP) and P(VdF-HFP)-based gel polymer electrolytes with different percentages of polymer contents. X-ray diffraction analysis shows the decrease of crystallinity of the gel polymer electrolytes in comparison to pure P(VdF-HFP). In general, PVdF is crystalline and shows its characteristic peaks at 2θ = 18.2, 20, 26.6 and 38. For P(VdF-HFP), three peaks are found at 2θ = 18.3, 20 and 26.5, which correspond well with the (1 0 0) + (0 2 0), (1 1 0) and (0 2 1) reflections of crystalline PVdF [24]. This is a confirmation of partial crystallization of the PVdF units in the copolymer to give an overall semi-crystalline morphology for P(VdF-HFP). In gel polymer electrolyte, only the prominent peak at

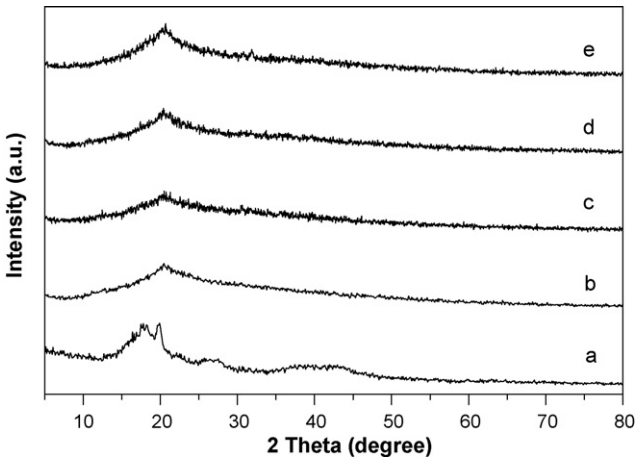

Fig. 1. XRD patterns of (a) P(VdF-HFP) and P(VdF-HFP)–(PC/DEC/ACN)–LiI-I_2–TBP electrolytes with different polymer contents (b) 4 wt%, (c) 6 wt%, (d) 8 wt% and (e) 10 wt%.

20° is observed and other peaks are decreased in intensity, which indicates the decrease in crystallinity. In the electrolyte systems with different percentages of polymer contents, it is observed that the peak intensity is minimum for 6 wt% of P(VdF-HFP) and then increased slowly with increase in polymer content. The decrement in peak intensity suggests an increase in the degree of amorphicity that helps in the migration of ions in the electrolyte system, which is responsible for enhancement of ionic conductivity.

3.2. ATR-FTIR spectroscopy

Infrared spectroscopy is a convenient method to provide the information about the chain structure of polymers and interactions of different groups in the P(VdF-HFP)–(PC/DEC/ACN)–LiI/I_2–TBP gel polymer electrolyte films. Fig. 2 displays the FTIR spectra of P(VdF-HFP) and gel polymer electrolyte systems with different percentages of polymer contents. It is clear that the spectrum of P(VdF-HFP) (Fig. 2a) contains peaks at wavenumbers 611, 760, 872, 972, 1064, 1180 and 1400 cm^{-1} that corresponds to vinylidene, CF_3 group, CH_2 wagging of the vinylidene band, out-of-plane C–H bending, –C–F– stretching, CF_2 stretching and scissoring vibration of the vinyl group, respectively [25,26]. The gel polymer electrolytes

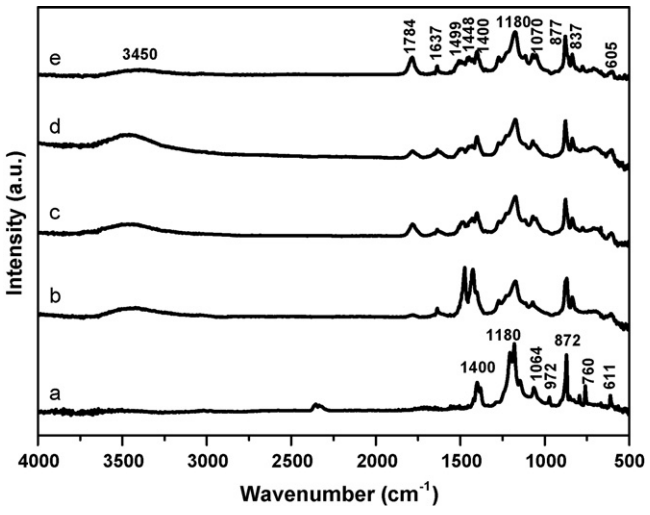

Fig. 2. ATR-FTIR spectra of (a) P(VdF-HFP) and GPE with different polymer contents (b) 4 wt%, (c) 6 wt%, (d) 8 wt% and (e) 10 wt%.

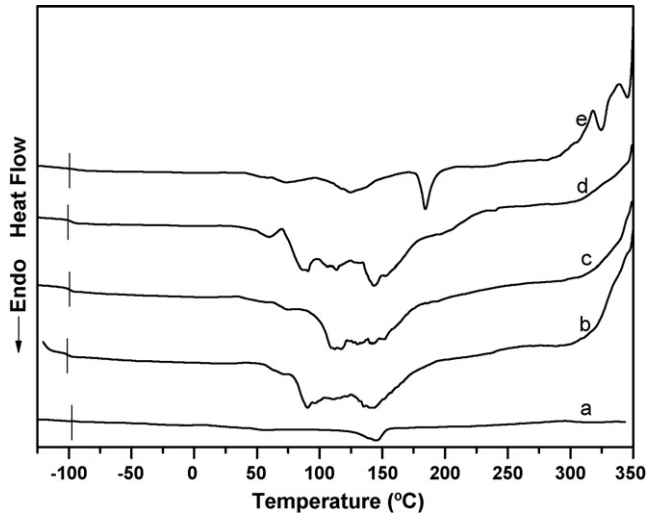

Fig. 3. DSC traces of (a) P(VdF-HFP) and GPE with different polymer contents (b) 4 wt%, (c) 6 wt%, (d) 8 wt% and (e) 10 wt%.

(Fig. 2b–e) show some additional peaks at 1780, 1637, 1499, 1448 and 837 cm^{-1}. The frequencies 1780 and 1637 cm^{-1} can be ascribed to the C=O stretching vibration of plasticizer, PC and DEC [27]. Frequencies 1499 and 1448 cm^{-1} are due to $-CH_3$ bending vibration of *tert*-butylpyridine. Frequency 837 cm^{-1} is due to CH_2 rocking vibration. The peaks at 872 and 611 cm^{-1} are shifted to 877 and 605 cm^{-1} in the electrolyte system, respectively. The broad band belonging to the –O–H stretching around 3600–3200 cm^{-1} suggests that a large number of intramolecular and intermolecular hydrogen bonds are formed by the interaction of PC/DEC and P(VdF-HFP). It is suggested that coordination and interaction of the solvents and salt with polymer may reduce the peak intensity to give amorphous structure to the gel polymer electrolytes. Also the different peak positions are shifted in the gel polymer electrolyte system. The shifting of peaks in the P(VdF-HFP)-based polymer electrolytes suggest the interaction among constituents of the polymer electrolyte.

3.3. DSC/TGA analysis

The overall thermal properties of the gel polymer electrolyte systems can be investigated by the DSC technique. The glass transition temperature, melting point and the thermal stability of the material are all important parameters resulting from the microstructure and morphology of the system. These parameters will affect the overall properties of the gel electrolyte material when operating in a dye-sensitized solar cell. The glass transition temperature (T_g) is one of the most important parameters of the amorphous phase for the flexibility of the polymer at room temperature. Fig. 3 shows DSC thermograms of pure P(VdF-HFP) and P(VdF-HFP)-based gel polymer electrolyte systems with different polymer contents. By assuming that pure PVdF is 100% crystalline, the relative percentage of crystallinity (X_c) is calculated based on the following equation with the DSC data.

$$X_c = \frac{\Delta H_m}{\Delta H_m^\circ} \times 100\%$$

where ΔH_m° is the standard enthalpy of fusion of pure PVdF, 105 J g^{-1} [28], and ΔH_m is enthalpy of fusion of the gel polymer electrolyte. T_g, X_c, ΔH_m and the crystalline melting temperature (T_m) for all GPE films are presented in Table 1 with varying polymer contents. From the Table 1 and Fig. 3, it is clear that glass transition temperature (T_g), melting temperature (T_m) and crystallinity (X_c)

Table 1
Thermal properties of gel polymer electrolyte system

Electrolyte samples	T_g (°C)	T_m (°C)	ΔH_m (J g^{-1})	X_c (%)
Pure P(VdF-HFP)	−98.3	145.2	42.9	40.85
S + 4 wt% P(VdF-HFP)	−101.0	140.7	22.7	21.61
S + 6 wt% P(VdF-HFP)	−100.2	142.4	9.23	8.79
S + 8 wt% P(VdF-HFP)	−101.2	143.4	14.3	13.61
S + 10 wt% P(VdF-HFP)	−99.2	183.5	30.1	28.66

S = (PC/DEC/ACN)–LiI-I_2–TBP

are decreasing in the electrolyte samples and then increases when the P(VdF-HFP) content is 10 wt% in the electrolyte system. The reorganization of polymer chain may hinder by the cross-linking centers formed by the interaction of the Lewis acid groups of salt with the polar groups of polymer. As a result, the degree of crystallization of polymer matrix decreases [29]. The crystallinity of the pure P(VdF-HFP) is found approximately 40%, while the crystallinity reduces up to 9% in the electrolyte samples. This facilitates the absorption of more liquid electrolyte to give an amorphous nature of the GPE sample. The decrease in T_g increases the flexibility of polymer chains, thus helps in fast ion conduction. The complicated, acid–base interactions between lithium, I^- in salt and fluorine in P(VdF-HFP) have occurred with the addition of polymer to the (PC/DEC/ACN)–LiI-I_2–TBP electrolyte system. Such interactions can not only induce structural modification of the polymer chain, which provides a favorable conduction path for faster migration of I^-/I_3^- ions, but also break the preformed crystals to render the polymer in the amorphous phase to some extent, which favors the improvement in conductivity [30,31]. Increased amount of P(VdF-HFP) (10 wt%) in electrolyte will induce crystalline site in the matrix which leads to lower segmental mobility.

The TGA curves of gel polymer electrolytes with varying polymer contents under nitrogen atmosphere are shown in Fig. 4. A continuous weight loss has occurred at low temperature in the gel polymer electrolyte because of the release of solvent and water. In case of pure P(VdF-HFP) 0.6% weight loss occurs due to vaporization of water. For GPE system, maximum only about 3% weight loss occurs at 80 °C mainly due to vaporization of ACN (bp 81 °C) and slightly because of PC and DEC. Although boiling point of PC and DEC are 242 and 126 °C, respectively, they evidently vaporize at low temperatures [32,33]. ACN gives the lowest device stability because it evaporates rapidly out of the P(VdF–HFP) films. But use of small amount of ACN with PC–DEC reduces the weight loss and

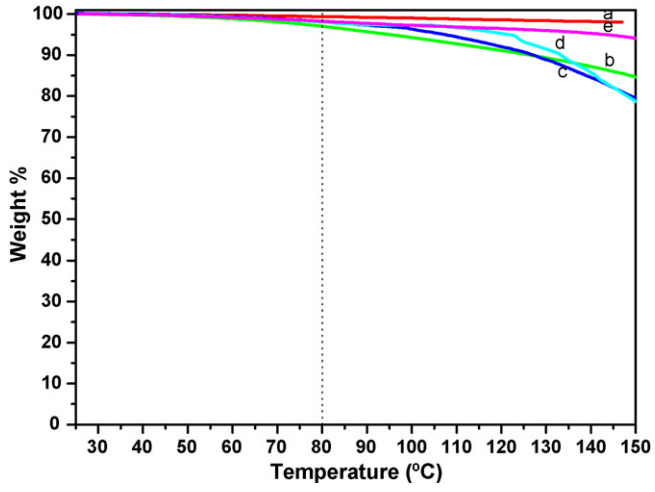

Fig. 4. TGA curves for (a) P(VdF-HFP) and GPE with different polymer contents (b) 4 wt%, (c) 6 wt%, (d) 8 wt% and (e) 10 wt%.

degradation of the cell and thereby making GPE based cells more thermally stable compared to liquid electrolyte cells.

3.4. SEM study

Fig. 5 presents SEM images of the nanoparticulate TiO_2 film on FTO glass and surface morphology of several gel polymer electrolytes on TiO_2 films with different percentages of polymer contents. The TiO_2 spherical nanoparticles are well distributed and the film has a porous structure in which the nanoparticles are all bonded together through a sintering process (Fig. 5a). Such a porous structure permits not only the adsorption of a greater number of dye molecules, but also better wetting of the electrolyte film. Together, these features result in a perfect penetration of the I^-/I_3^- redox couple into the TiO_2 film. For the electrolyte samples, the film with 4 wt% P(VdF-HFP) seems to be almost non-porous which is responsible for low ionic conductivity. The porosity of the films increases with increase of P(VdF-HFP) content up to 8 wt% and then slightly decreases. The increased porosity in the GPE leads to the entrapment of large volumes of the liquid electrolyte in the cavities accounting for the increased ionic conductivity. Surface morphology implies the penetration of polymer electrolyte into the dye-sensitized nanopores, which leads to effective reduction of the dye cation by iodide ions in the polymer electrolyte. The increased ionic conductivity reveals the faster movement of I^-/I_3^- in the electrolyte and thus improves the photovoltaic performance.

3.5. Ionic conductivity measurements

The ionic conductivity of gel polymer electrolytes is calculated from $\sigma = L/(R_b A)$, where L and A represent thickness of the electrolyte specimen and area of the electrode, respectively. R_b is the bulk resistance of the gel electrolyte obtained from complex impedance measurements. Fig. 6 shows the conductivity versus temperature inverse plots of the gel polymer electrolyte systems with varying polymer contents. It is observed that the logσ versus $1/T$ plots are linear, suggesting that the temperature dependence of ionic conductivity obeys the "Arrhenius" equation:

$$\sigma = \sigma_0 \exp\left(\frac{-E_a}{kT}\right)$$

where σ_0 is the pre-exponential factor, E_a is the activation energy and k is the Boltzmann constant. From the slopes of the plots E_a values of electrolytes with different concentration of P(VdF-HFP) polymer are evaluated and found in the range of 1.61 to 2.51 J mol^{-1}. The minimum value of E_a of 1.61 J mol^{-1} is found for 8 wt% polymer content. Very low value of E_a suggests that ionic conduction is facile in the polymer electrolyte. The behavior of conductivity enhancement with temperature can be understood in terms of the free-volume model [34]. As the temperature increases, the polymer can expand easily and produce free volume. Thus, as temperature increases, the free volume increases. Also rise in temperature improves the dissociation of salt. The resulting conductivity, represented by the overall mobility of ions and the polymer, is determined by the free volume around the polymer chains. Therefore, as temperature increases, ions, solvated molecules, or polymer segments can move into the free volume. This leads to an increase in ion mobility and segmental mobility that will assist ion transport and virtually compensate for the retarding effect of the ion clouds.

From the plot it is observed that the ionic conductivity increases with the increase in polymer content up to 8 wt% and decreases further when the concentration is increased. The highest room temperature (30 °C) ionic conductivity is found to be 5.25×10^{-3} S cm^{-1} for 8 wt% of polymer content. It is known that

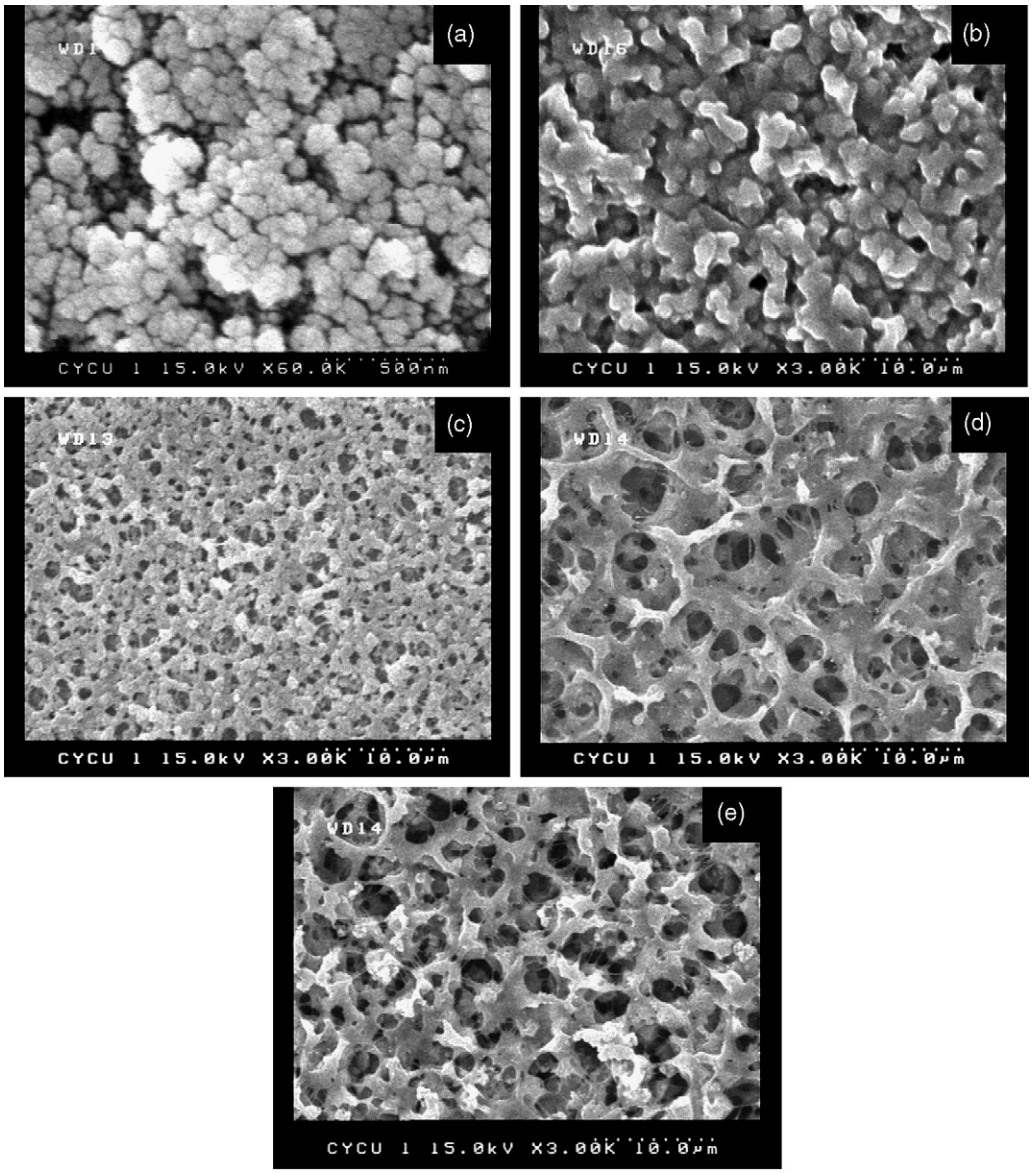

Fig. 5. SEM images of (a) TiO_2 nanoparticles film on FTO glass and P(VdF-HFP)–(PC/DEC/ACN)–LiI-I_2–TBP electrolytes on TiO_2 film with different polymer contents (b) 4 wt%, (c) 6 wt%, (d) 8 wt% and (e) 10 wt%.

gel polymer electrolyte is formed by trapping liquid electrolyte in polymer cavities. With the addition of larger amount of polymer in gel polymer electrolyte, the cavities in gel polymer electrolyte become smaller which result in hindering ionic movement, so the ionic conductivity decreases above 8 wt% polymer content. Another reason of reduction in conductivity is viscosity. With the accretion of the P(VdF-HFP) concentration, the viscosity of the electrolytes increases, which decreases the mobility of the charge carriers and hence intends to reduce the ionic conductivity. At low P(VdF-HFP) concentration, the initial increase in the ionic conductivity is attributed to the build-up of charge carriers. At high P(VdF-HFP) concentrations, the build-up of charge carriers is offset by the retarding effect of ionic clouds and the viscosity of the electrolytes rises up largely, resulting in the decrease in ionic conductivity [35].

It is generally accepted that ionic conductivity in polymer electrolytes is mainly attributed to a property of amorphous phase above their glass transition temperatures. The interaction of LiI/I_2 with P(VdF-HFP) segments results in the structural modification of the polymer chain, thereby providing a favorable conduction path for the faster migration of I^-/I_3^- ions in the electrolyte. On the other hand, however, the interaction of LiI/I_2, PC/DEC and P(VdF-HFP) decreases the crystalline phase in the polymer. The restriction of crystallization and the increase of the amorphous phase favor the improvement of ionic mobility and conductivity.

3.6. Photovoltaic performance

Fig. 7 shows the *J–V* curves of dye-sensitized solar cells (DSSCs) recorded under the illumination of 100 mW cm^{-2}. The photovoltaic properties derived from Fig. 7 are summarized in Table 2. The DSSC assembled with the gel polymer electrolyte reports a lower short circuit density (J_{SC}) and higher/similar open circuit voltage (V_{OC}) than the DSSC with a liquid electrolyte. The lower value of J_{SC} in the DSSC with gel polymer electrolyte may originate from its lower ionic conductivity than liquid electrolyte. A higher resistance to ion migration reduces the supply of I_3^- to the Pt counter-electrode. This causes reduction of I_3^- and also retards the kinetics of dye regeneration, and therefore, decreases the J_{SC}. The increase in the

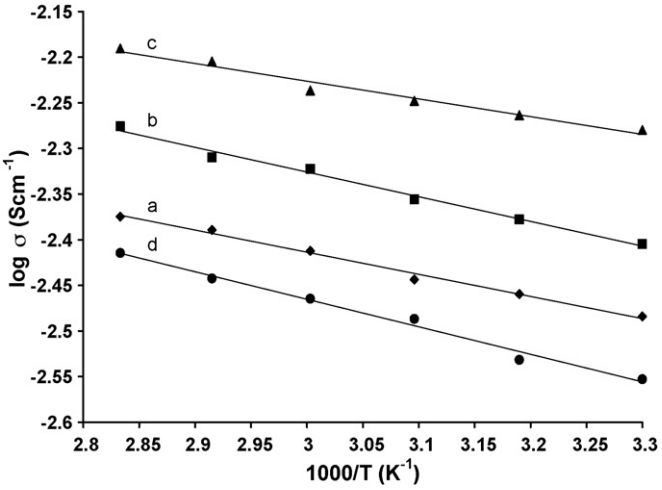

Fig. 6. Temperature dependence of ionic conductivity of P(VdF-HFP)–(PC/DEC/ACN)–LiI-I_2–TBP electrolytes with different polymer contents (a) 4 wt%, (b) 6 wt%, (c) 8 wt% and (d) 10 wt%.

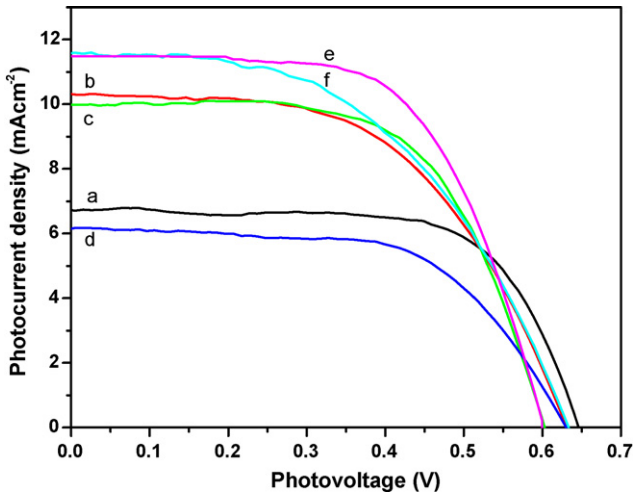

Fig. 7. Photocurrent–voltage characteristics of Nanocrystalline TiO_2 photoelectrochemical cell with GPE electrolytes with different polymer contents (a) 4 wt%, (b) 6 wt%, (c) 8 wt%, (d) 10 wt%, (e) sample (c) with N719 dye and (f) liquid electrolyte without polymer.

viscosity can reduce the diffusion rate of I_3^- in the electrolyte and hence affect the performance of cells, especially J_{SC} [36]. Therefore, comprehensively influenced by both the conductivity and viscosity of P(VdF-HFP) gel electrolyte, the optimum photoelectrochemical performance is achieved at P(VdF-HFP) concentration of 8 wt%. The slight increase of V_{OC} for the DSSC with gel polymer electrolyte is related to the reduction of the back electron-transfer reaction that decreases the V_{OC} [12]. The maximum energy conversion efficiency (η) of 3.95% with 8 wt% P(VdF-HFP) content is obtained using N3 dye. This improvement in efficiency compared to other compositions may be ascribed to the higher electrolyte conductivity and faster dye regeneration rate due to weaker ion-pairing. The fill factor (FF) improvement of the GPE cells in comparison to liquid electrolyte cell is due to the considerable interfacial contact and a high ionic conductivity, which is beneficial for reducing the inner resistance of the whole cell. It is well known that fluorine, which is present in P(VdF-HFP), has the smallest ionic radius and the largest electronegativity, repelling electrons. This is favorable for suppressing the dark current at the semiconductor/electrolyte interface, reducing the recombination rate and improves the ionic transport when applied in dye-sensitized nanocrystalline solar cells [37].

Table 2
Performance characteristics of DSSCs at 100 mW cm^{-2}

Electrolyte samples	V_{OC} (V)	J_{SC} (mA cm^{-2})	FF	η (%)
Liquid electrolyte, (PC/DEC/ACN-LiI-I_2-TBP)	0.64	11.54	0.51	3.77
S + 4 wt% P(VdF-HFP)	0.65	6.43	0.77	3.22
S + 6 wt% P(VdF-HFP)	0.64	10.31	0.55	3.63
S + 8 wt% P(VdF-HFP)	0.61	9.95	0.65	3.95
S + 10 wt% P(VdF-HFP)	0.64	6.03	0.63	2.43
S + 8 wt% P(VdF-HFP), N719 dye	0.6	11.48	0.64	4.41

To know the dye performance on the conversion efficiency, the highest efficiency cell of 8 wt% P(VdF-HFP) content is tested with N719 dye. With N719 dye the conversion efficiency is increased up to 4.41%. In N3 dye, hydrogen bonding induces dye aggregation in solution and in the adsorbed state. However due to the deprotonation of two carboxylic groups, N719 dye has less tendency to undergo aggregation [38,39]. The bulky tetrabutylammonium (TBA) groups of N719 prohibit the aggregation. Aggregation of sensitizer dyes on nanocrystalline semiconductor films has been reported to reduce solar cell performance [40]. It has been found that the electron injection rate is suppressed by the aggregation of N3 dye molecules on TiO_2 nanocrystalline films. So the performance of the cell with N719 dye is better than N3 dye.

4. Conclusions

The P(VdF-HFP)/PC/DEC based gel polymer electrolytes are synthesized and successfully employed to regenerative photoelectrochemical cells that yielded maximum conversion efficiency of about 3.95% to 4.41% with N3 and N719 dye, respectively, for 8 wt% polymer content. Aggregation of N3 dye on TiO_2 electrode is responsible for the reduction in efficiency in comparison to N719 dye. It is found that the ionic conductivity of gel polymer electrolyte plays a crucial role on short-circuit current density. The optimized concentration of 8 wt% polymer makes the GPE more flexible and porous that improves solvent retention capacity resulting higher ionic conductivity of the electrolyte. The presence of fluorine in P(VdF-HFP) reduces the recombination rate and increases the fill factor, making the conversion efficiency of GPE comparable to liquid electrolyte cell.

Acknowledgements

The authors gratefully acknowledge the support of the Center-of-Excellence Program on Membrane Technology, the Ministry of Education, Taiwan, ROC, and that of Chung Yuan Christian University (grant no. CYCU-95-CR-CH) to carry out the research work.

References

[1] B. O'Regen, M. Grätzel, Nature 353 (1991) 737.
[2] Z.G. Chen, Y.W. Tang, L.S. Zhang, L.J. Luo, Electrochim. Acta 51 (2006) 5870.
[3] M. Grätzel, J. Photochem. Photobiol. A 168 (2004) 235.
[4] P. Ravirajan, A.M. Peiro, M.K. Nazeeruddin, M. Grätzel, D.D.C. Bradley, J.R. Durrant, J. Nelson, J. Phys. Chem. B 110 (2006) 7635.
[5] M. Grätzel, Inorg. Chem. 44 (2005) 6841.
[6] Z.G. Chen, F.Y. Li, H. Yang, T. Yi, C.H. Huang, Chem. Phys. Chem. 8 (2007) 1293.
[7] P. Wang, S.M. Zakeeruddin, P. Comte, I. Exnar, M. Grätzel, J. Am. Chem. Soc. 125 (2003) 1166.
[8] H. Yang, C.Z. Yu, Q.L. Song, Y.Y. Xia, F.Y. Li, Z.G. Chen, X.H. Li, T. Yi, C.H. Huang, Chem. Mater. 18 (2006) 5173.
[9] Z. Lan, J.H. Wu, J.M. Lin, M.L. Huang, J. Power Sources 164 (2007) 921.
[10] F.J. Li, F.Y. Cheng, J.F. Shi, F.S. Cai, M. Liang, J. Chen, J. Power Sources 165 (2007) 911.

[11] J.B. Xia, F.Y. Li, C.H. Huang, J. Zhai, L. Jiang, Sol. Energy Mater. Sol. Cells 90 (2006) 944.
[12] D.W. Kim, Y.B. Jeong, S.H. Kim, D.Y. Lee, J.S. Song, J. Power Sources 149 (2005) 112.
[13] P. Wang, S.M. Zakeeruddin, J.E. Moser, M.K. Nazeeruddin, T. Sekiguchi, M. Grätzel, Nat. Mater. 2 (2003) 402.
[14] J.H. Kim, M.-S. Kang, Y.J. Kim, J. Won, N.-G. Park, Y.S. Kang, Chem. Commun. (2004) 1662.
[15] M.-S. Kang, J.H. Kim, Y.J. Kim, J. Won, N.-G. Park, Y.S. Kang, Chem. Commun. (2005) 889.
[16] T. Stergiopoulos, I.M. Arabatzis, G. Katsaros, P. Falaras, Nano Lett. 2 (2002) 1259.
[17] W. Kubo, Y. Makimoto, T. Kitamura, Y. Wada, S. Yanagida, Chem. Lett. (2002) 948.
[18] S. Anandan, S. Pitchumani, B. Muthuraaman, P. Maruthamuthu, Sol. Energy Mater. Sol. Cells 90 (2006) 1715.
[19] A.F. Nogueira, C. Longo, M.-A. De Paoli, Coord. Chem. Rev. 248 (2004) 1455.
[20] F.R.F. Fan, H.Y. Liu, A.J. Bard, J. Phys. Chem. 89 (1985) 4418.
[21] R. Dabestani, X.L. Wang, A.J. Bard, A. Campion, M.A. Fox, S.E. Webber, J.M. White, J. Phys. Chem. 90 (1986) 2729.
[22] L. Kavan, M. Grätzel, Electrochim. Acta 34 (1989) 1327.
[23] J. Wu, Z. Lan, J. Lin, M. Huang, S. Hao, L. Fang, Electrochim. Acta 52 (2007) 7128.
[24] D. Saikia, A. Kumar, Electrochim. Acta 49 (2004) 2581.
[25] R.M. Silverstein, F.X. Webster, Spectroscopic Identification of Organic Compounds, 6th edition, John Wiley and Sons, New York, USA, 1997, Chapter 3.
[26] D.L. Pavia, G.M. Lampman, G.S. Kriz, Introduction to Spectroscopy, Harcourt College Publication, USA, 2001, Ch. 2.
[27] J. Wu, S. Hao, Z. Lan, J. Lin, M. Huang, Y. Huang, L. Fang, S. Yin, T. Sato Adv. Funct. Mater. 17 (2007) 2645.
[28] B. Wunderlich, Macromolecular Physics, vol. 3, Academic Press, 1980, p. 50.
[29] B.J. Ash, L.S. Schadler, R.W. Siegel, Mater. Lett. 55 (2002) 83.
[30] C.-Y. Chiang, M. Jaipal Reddy, P.P. Chu, Solid State Ionics 175 (2004) 631.
[31] C.W. Lin, C.L. Hung, M. Venkateswarlu, B.J. Hwang, J. Power Sources 146 (2005) 397.
[32] K.S. Kim, S.Y. Park, S. Choi, H. Lee, J. Power Sources 155 (2006) 385.
[33] M.S. Ding, J. Electrochem. Soc. 150 (4) (2003) A455.
[34] S. Rajendran, T. Uma, J. Power Sources 88 (2000) 282.
[35] W. Li, J. Kang, X. Li, S. Fang, Y. Lin, G. Wang, X. Xiao, J. Photochem. Photobiol. A 170 (2005) 1.
[36] W. Kubo, S. Kambe, S. Nakade, T. Kitamura, K. Hanabusa, Y. Wada, S. Yanagida, J. Phys. Chem. B 107 (2003) 4374.
[37] H. Han, W. Liu, J. Zhang, X.-Z. Zhao, Adv. Funct. Mater. 15 (2005) 1940.
[38] B. Wenger, M. Grätzel, J.-E. Moser, J. Am. Chem. Soc. 127 (2005) 12150.
[39] M. Murai, A. Furube, M. Yanagida, K. Hara, R. Katoh, Chem. Phys. Lett. 423 (2006) 417.
[40] S. Kambe, K. Murakoshi, T. Kitamura, Y. Wada, S. Yanagida, H. Kominami, Y. Kera, Sol. Energy Mater. Sol. Cells 61 (2000) 427.